Determination of localized surface phonons in nanocrystalline silicon by inelastic neutron scattering spectroscopy and its application to deuterium isotope enrichment

Takahiro Matsumoto [1,2,*] Ikumi Nomata,[2] Takashi Ohhara [3] and Yoshihiko Kanemitsu [4]

[1]*Graduate School of Design and Architecture, Nagoya City University, Nagoya 464-0083, Japan*
[2]*Graduate School of Medical Sciences, Nagoya City University, Nagoya 464-0083, Japan*
[3]*Neutron Science Section, J-PARC Center, Japan Atomic Energy Agency, Ibaraki 319-1195, Japan*
[4]*Institute for Chemical Research, Kyoto University, Uji, Kyoto 611-0011, Japan*

(Received 27 October 2020; revised 5 April 2021; accepted 26 May 2021; published 28 June 2021)

The hydrogen (H) isotope deuterium (D) has attracted special interest for the manufacture of silicon (Si) semiconductors, Si microchips, and optical fibers, as well as for the synthesis of isotopically labeled compounds. However, the efficient production of D or H deuteride in a controlled manner is challenging, and rational H isotope enrichment protocols are still lacking. Here, we demonstrate a highly efficient exchange reaction from H to D on the surface of nanocrystalline Si (n-Si). Fourfold enrichment of D termination was successfully achieved by dipping n-Si into a dilute D solution. By determining the surface-localized vibrational modes for H- and D-terminated n-Si using inelastic neutron scattering spectroscopy, we found that the physical mechanism responsible for this enrichment originates from the difference in the zero-point oscillation energies and entropies of the surface-localized vibrations. Theoretically, the extent of enrichment could be greatly enhanced (∼15 times) using a gas-phase reaction. This enrichment protocol, which avoids the use of precious metal catalysts, opens the way for sustainable H-to-heavy H exchange reactions.

DOI: 10.1103/PhysRevMaterials.5.066003

I. INTRODUCTION

Hydrogen (H) isotopes such as deuterium (D) are trace components of naturally occurring molecular H and have applications as fine chemicals owing to their unique physical, quantum, and nuclear properties [1]. Because of its large mass difference, nonradioactive nature, and stable characteristics, D is often employed for the synthesis of diverse D-labeled compounds that have been recognized as indispensable research tools in the life, environmental, and material sciences.

In semiconductor technologies, specificity differences between H and D can be observed on metal or semiconductor surfaces. Fundamental scanning tunneling microscopy studies [2,3] have revealed that a D-terminated silicon surface (Si-D) has a lower probability for desorption (∼100-fold) than a H-terminated silicon surface (Si-H) [4,5]. Although the physical mechanism responsible for this large isotope effect remains an open question, the quantum coupling of the bending modes of Si-D to the bulk Si phonon is considered to play an important role in desorption and adsorption processes [6–8]. This discovery inspired the idea of passivating Si-dangling bonds with D instead of H, which is greatly beneficial because D passivation significantly extends and improves the cycle life of Si semiconductors, microchips, and solar cells [9–14].

Despite the many promising applications of D atoms, D reagents have conventionally been produced by electrolysis, which requires large amounts of energy [15]; therefore, commercially available reagents are not cost competitive. Other methods, such as the reactions of various metals, have traditionally been employed to generate D atoms on the laboratory scale. These reagents have some drawbacks, as they are toxic, produce large amounts of waste, and require high reaction temperatures [16]. To overcome these disadvantages, a number of metal-catalyzed H-D exchange reactions based on rare transition metals [17–21] or transition metal compounds [22–24] have been developed to synthesize D-labeled compounds. However, as these reactions require scarce resource rare metals, various issues need to be resolved to realize sustainable, economical, and environmentally friendly D enrichment protocols.

Here, we report an efficient exchange reaction from H to D termination on the surface of nanocrystalline Si (n-Si). We achieved fourfold enrichment of D termination using a dilute D solution. To precisely estimate the reaction rates, the zero-point energies of the localized vibrational modes were identified using inelastic neutron scattering (INS) spectroscopy, which can provide crucial information on the localized vibrational dynamics of H or D nuclei [25–28]. Based on the surface-localized vibrational modes for H- and D-terminated n-Si, as determined using INS spectroscopy, we found that the physical mechanism of the observed enrichment originates from the difference in the zero-point oscillation energies and entropies of the surface-localized vibrations. The configuration free energy for reaction activation was derived from quantum mechanically calculated internal energies and entropies (QMCIE) based on these localized vibrational modes. This calculation revealed that the extent of enrichment could be greatly enhanced (∼15 times) using a gas-phase reaction.

*Corresponding author: matsumoto@sda.nagoya-cu.ac.jp

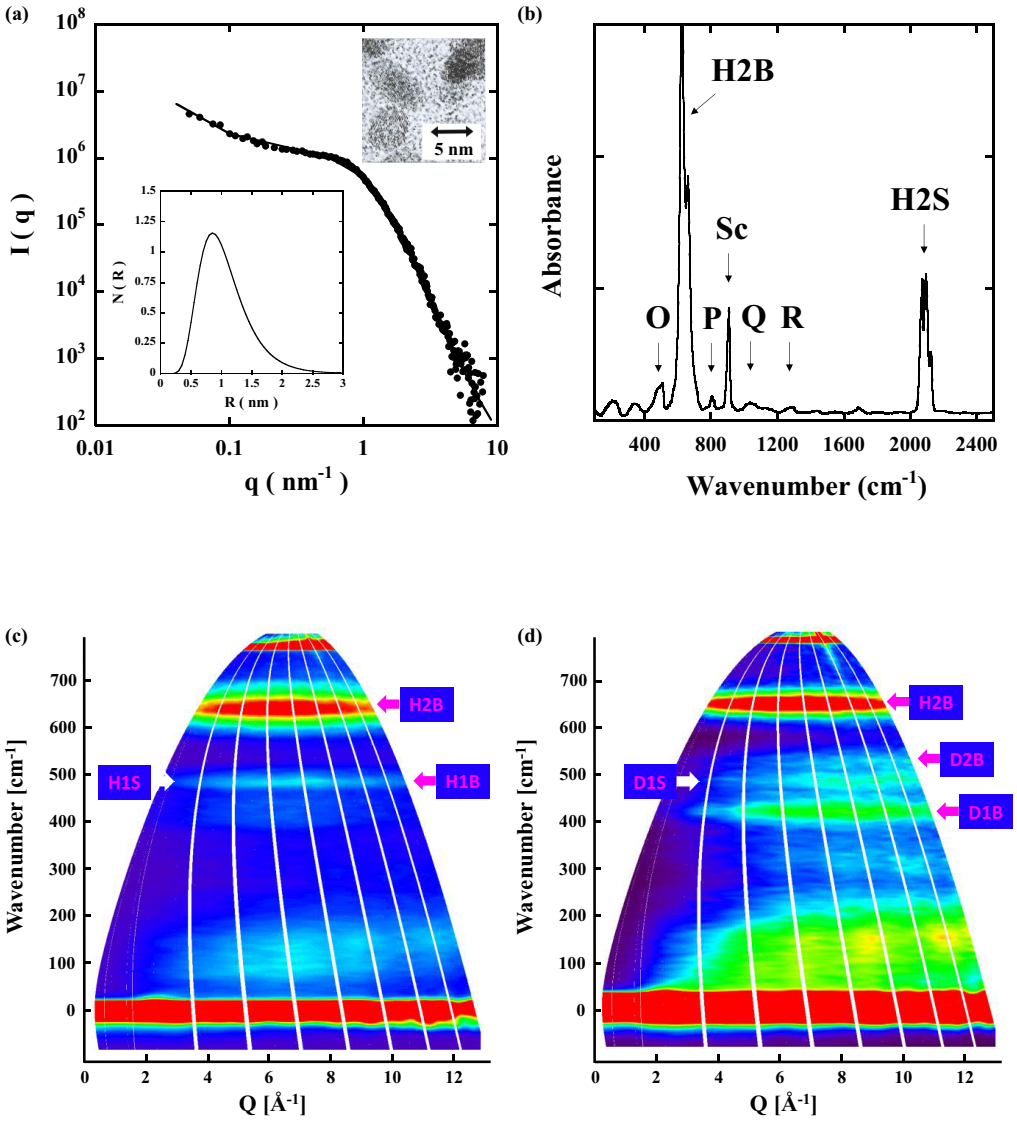

FIG. 1. Nanostructure characterization. (a) Small-angle x-ray scattering (SAXS) intensity (solid circles), size distribution (lower inset), and lattice image obtained by transmission electron microscopy (TEM) analysis (upper inset). (b) Infrared phonon and Si-H vibrational spectrum obtained by Fourier transform infrared (FTIR) measurement. Localized vibrational modes for (c) n-Si:H and (d) n-Si:D obtained by inelastic neutron scattering (INS) spectroscopy. B and S denote bending and stretching modes, respectively. The broad band observed between 0 and 20 meV originates from acoustic Si phonons.

II. NANOSTRUCTURE FABRICATION AND CHARACTERIZATION

A. Electrochemical anodization and nanostructure core characterization

Here, n-Si films were formed by electrochemical anodization [29,30]. All samples were formed on *p*-type (100) oriented crystalline Si wafers with resistivities of 3–5 Ω cm. Thin Al films were evaporated on the back of the wafers to form a good ohmic contact, and a platinum mesh was used for the anodization cathode. The film was fabricated in the dark to avoid oxidation using a hydrofluoric acid (HF)-ethanol solution ($HF/H_2O/C_2H_5OH = 25 : 45 : 30$, volume ratio; ultrahigh-purity HF acid supplied by Stella Chemifa Corporation, Japan) by applying a positive bias to the substrate with a constant current density in the range of 10 mA/cm^2 for 60 min. The D-terminated n-Si films (n-Si:D) were prepared in the same manner using deuterated electrolyte solutions.

Figure 1(a) shows the results of small-angle x-ray scattering (SAXS) measurements. The SAXS intensity $I(q)$ (circles) as a function of wave number q(nm^{-1}) determined for the n-Si films provides information on the size distribution and the average radius of the n-Si film. The lower inset in Fig. 1(a) shows the size distribution $N(R)$, which was determined from the theoretically fitted SAXS intensity curve (solid line) obtained using a polydisperse hard spherical nanocrystalline model [30,31]. The average radius was estimated to be 1.05 nm. We also evaluated the crystallinity by transmission electron microscopy (TEM) analysis, and the lattice image is shown in the upper inset of Fig. 1(a). The lattice image of n-Si reveals an atomic spacing of 0.3 nm, which corresponds to the Si (111) interplanar spacing.

B. Characterization of nanostructure surface termination by Fourier transform infrared and INS spectroscopies

Figure 1(b) shows the infrared phonon and Si-H vibrational spectrum obtained by Fourier transform infrared (FTIR) measurements. Generally, FTIR probes the electric dipole moment, which is larger at the surface of n-Si than in the n-Si lattice core; therefore, Si-H vibrational modes show stronger absorbance than optical phonon modes. For example, optical phonon bands (O = 500 cm^{-1}) show weak absorbance. In contrast, the Si-H bending mode (H2B = 650 cm^{-1}), Si-O-H bending mode (P = 800 cm^{-1}), H-Si-H scissor mode (Sc = 905 cm^{-1}), Si-O-Si stretching mode (Q = 950–1150 cm^{-1}), C-H deformation mode (R = 1250 cm^{-1}), and $Si-H_X$ stretching modes (H2S : $Si-H$ = 2075 cm^{-1}, $Si-H_2$ = 2090 cm^{-1}, and $Si-H_3$ = 2125 cm^{-1}) show strong absorbance. No absorbance was observed in the region of 1500 cm^{-1}(= 2100 $cm^{-1}/\sqrt{2}$). Therefore, when H atoms are replaced by D atoms during the exchange reaction between Si-H and HDO, clear evidence of this reaction should be observable in this spectral region.

It should be noted that the overlap between various phonon modes such as bulk Si phonons and surface vibrations in the low energy region <800 cm^{-1} prevents clear resolution and spectral assignment of the surface vibrations using FTIR spectroscopy [32,33]. In contrast, INS spectroscopy provides clear spectra for the Si-H and Si-D vibrations as well as the bulk Si phonons because both the cross-sections (σ_H = 82.02 barn, σ_D = 7.64 barn, and σ_{Si} = 2.12 barn [34]) and momentum transfer dependence (originating from the difference in mass) are significantly different for these atoms (Si, H, and D). Therefore, we determined the surface vibrations for both Si-H and Si-D (bending and stretching modes) by INS spectroscopy.

INS measurements were performed for the n-Si:H and n-Si:D films using a time-of-flight (TOF) MARI chopper spectrometer at the ISIS Facility at the Rutherford Appleton Laboratory. We measured the contour plots of the dynamic structure factor $S(Q, \hbar\omega)$ [scattering intensity (S), energy ($\hbar\omega$), and momentum-transfer (Q) axis] for n-Si at 50 K with an incident neutron energy E_i of 0.1 eV. Figures 1(c) and 1(d) show the contour plots of the scattering intensity $S(Q, \hbar\omega)$ as a function of momentum transfer Q and energy $\hbar\omega$ for n-Si:H and n-Si:D, respectively. Here, the momentum transfer vector $\boldsymbol{Q}$ is defined as $\boldsymbol{Q} = \boldsymbol{k}_i - \boldsymbol{k}_f (Q = |\boldsymbol{k}_i - \boldsymbol{k}_f|)$ with $k_i = 2\pi/\lambda_i$ and $k_f = 2\pi/\lambda_f$, where λ_i and λ_f are the incident and scattered wavelengths, respectively. The neutron energy transfer is $E = \hbar\omega$. The inelastic scattering peaks at the energy levels of $\hbar\omega$ = 650 cm^{-1} [H2B: dominated by H motion (80%)] and 485 cm^{-1} [H1B: dominated by Si motion (80%), and H1S: dominated by Si motion (96%)] in Fig. 1(c) can be assigned to higher (H2B) and lower (H1B) energy bending vibrations of the XY plane and a lower energy stretching vibration (H1S) in the Z direction. The higher energy stretching vibration has an energy of 2100 cm^{-1} [H2S: dominated by H motion (96%)], as shown in the FTIR spectrum in Fig. 1(b). The above percentages were determined using the weight (coefficient) of the Si-H normal modes. The peak position of these vibrational levels is Q = 6.5 $Å^{-1}$, whereas the peak positions of the longitudinal optical and transverse optical phonon states are $Q \geqslant 13$ $Å^{-1}$ (not shown). Furthermore, the higher order energy levels of these states (H1B, H2B, and H2S) were found to be equally separated by $n\hbar\omega$ (n: integer) [35]. Therefore, these localized surface vibrations can be described by the six freedom of Si-H normal modes, and the harmonic oscillators quantitatively express the H dynamics in coordination with the Si motion with an energy of $E_i^{(H)} = [n_i^{(H)} + 1/2]\hbar\omega_i^{(H)}$, where subscript i denotes the type of vibrational mode.

Figure 1(d) shows the contour plot for n-Si:D. In addition to the spectrum originating from the H vibration (H2B), spectra are clearly observed at energy levels of $\hbar\omega$ = 540 cm^{-1} [D2B: dominated by Si motion (80%)], 485 cm^{-1} [D1S: dominated by Si motion (92%)], and 410 cm^{-1} [D1B: dominated by D motion (80%)]. The higher energy stretching vibration has an energy of 1525 cm^{-1} [D2S: dominated by D motion (92%)], as shown in the FTIR spectrum in Fig. 2(b). These spectral modes coincide with the eigenenergies of Si-D normal mode oscillation. The scattering originating from H or D atoms can be understood based on the peak positions in the energy-sliced spectrum as a function of Q. The peak position of the vibrational levels originating from D atoms is Q = 8.0 $Å^{-1}$, which is quite different from that of the vibrational levels originating from H atoms (Q = 6.5 $Å^{-1}$). These spectra and the energies are well described by harmonic oscillators with the same force constant as H. Thus, the energy levels of Si-D vibrations can be expressed as $E_i^{(D)} = [n_i^{(D)} + 1/2]\hbar\omega_i^{(D)}$. Here, we note that the scattering cross-section of the H atoms in the INS measurements is >10 times larger than that of the D atoms ($\sigma_{scatt}{}^{(D)}/\sigma_{scatt}{}^{(H)} \approx 7.64/82.03$ [34]); therefore, despite the lower concentration of H atoms (<10%), the Si-H mode results in an intense $S(Q, \hbar\omega)$ spectrum, as shown by the H2B mode in Fig. 1(d). The energies of the stretching and bending modes for the Si-H and Si-D vibrations are summarized in Table I. For comparison, Table I also includes previously calculated and observed values for the Si-H and Si-D vibrational energies [33,35–39]. Few data are available for the Si-D vibrational frequencies, especially for the Si-D bending modes [33,36,37]; however, both the Si-H and Si-D vibrational frequencies obtained here are 1–3% higher than those theoretically calculated for a Si(111) surface [38,39]. We consider this difference to be due to the relaxed surface structure with various crystal planes in n-Si.

C. Preparation of standard samples and evaluation of D ratio by TOF secondary ion mass spectrometry and FTIR measurements

Before performing D enrichment experiments, we prepared 0, 5, 10, 15, and 20% deuterated n-Si thin films via anodization using D_2O (0, 5, 10, 15, and 20%) in a mixed HF-ethanol solution. These films constituted standard samples to determine the ratio of D termination. We evaluated the ratio of D termination for these standard samples by FTIR spectroscopy and TOF secondary ion mass spectrometry (SIMS). Here, the TOF-SIMS depth profile from the surface to a depth of 1 μm was obtained by sputtering the film with 2 keV Cs^+ over a 500 × 500 μm region. We used a 30 keV Bi^{3+} beam operated at 0.5 μA for the primary ion. Figure 2(a) shows the attenuated total reflectance (ATR) spectra of the 0%-deuterated (blue line), 10%-deuterated (green line), and 20%-deuterated (red line) n-Si thin films in the wave

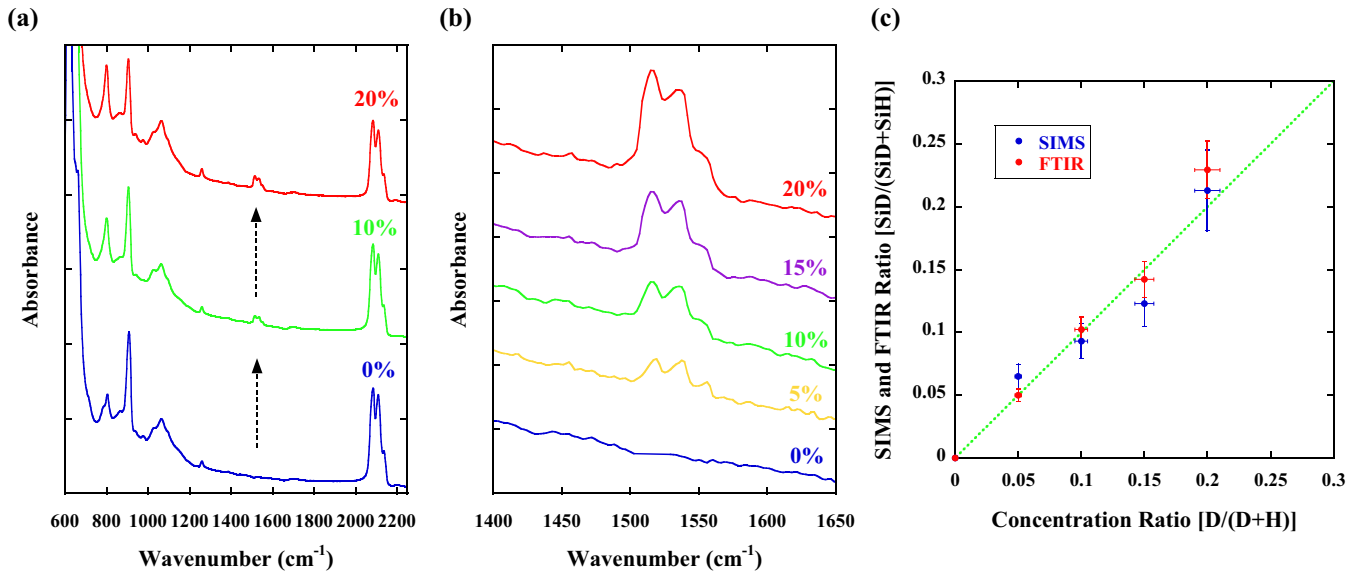

FIG. 2. Fourier transform infrared (FTIR) and secondary ion mass spectrometry (SIMS) measurements. (a) Attenuated total reflectance (ATR) spectra of 0% (blue line), 10% (green line), and 20% (red line) deuterated n-Si thin films. (b) Detailed ATR spectra of Si-D stretching modes (0%: blue line, 5%: yellow line, 10%: green line, 15%: purple line, 20%: red line). (c) Correlation between the D termination ratio [SiD]/([SiD] + [SiH]) and the D_2O concentration in the anodization electrolyte (0, 5, 10, 15, or 20%), as evaluated by ATR (red circles) and SIMS (blue circles) measurements.

number region from 600 to 2300 cm^{-1}. The spectra exhibit Si-H bending (650 cm^{-1}), Si-O-H bending (800 cm^{-1}), H-Si-H scissor (905 cm^{-1}), Si-O-Si stretching (950–1150 cm^{-1}), C-H deformation (1250 cm^{-1}), Si-D stretching (1480–1570 cm^{-1}), and Si-H stretching (2000–2200 cm^{-1}) modes. The intensity of the Si-D stretching mode (1480–1570 cm^{-1}) increased with increasing concentrations of D_2O in the HF-ethanol solution, whereas the intensity of the Si-H stretching mode (2000–2200 cm^{-1}) decreased. A strong absorption band for the Si-D bending mode, which overlaps with the bulk Si phonon and the Si-H bending modes, could not be clearly observed in the FTIR measurements.

Detailed ATR spectra for the Si-D stretching mode are shown in Fig. 2(b). This spectral mode, which increases with increasing D_2O concentration in the HF-ethanol solution (0%: blue line, 5%: yellow line, 10%: green line, 15%: purple line, 20%: red line), is composed of three peaks: Si-D stretching (1515 cm^{-1}), $Si-D_2$ stretching (1535 cm^{-1}), and $Si-D_3$ stretching (1557 cm^{-1}). Here, we note that the relative intensities of these three peaks show a weak dependence on the D_2O concentration. This result indicates that $Si-D_2$ has a more stable configuration energy than Si-HD and that the surface termination structure changes slightly depending on the D_2O concentration.

The proportion of D in each sample was analyzed based on the total spectral area of these Si-D stretching modes vs that of the Si-H stretching modes. The oscillator strength and the spectral sensitivity of the Si-H and Si-D stretching modes are different. Therefore, to compare the ratio of D in n-Si determined by FTIR with the D_2O concentration, the Si-D absorbance was calibrated using $N_D/(N_H+N_D) = \eta\int_{\omega_D}\frac{\alpha(\hbar\omega)}{\hbar\omega}d(\hbar\omega)/[\int_{\omega_H}\frac{\alpha(\hbar\omega)}{\hbar\omega}d(\hbar\omega)+\eta\int_{\omega_D}\frac{\alpha(\hbar\omega)}{\hbar\omega}d(\hbar\omega)]$, where η values of 2.8 and 1.4 were chosen for ATR-FTIR and reflection-FTIR (R-FTIR) measurements, respectively. These values were evaluated based on the previously reported FTIR absorbance for fully D-terminated n-Si films [32,33,40–42].

Based on the values estimated by ATR (red circles) and SIMS (blue circles), a correlation curve between the D termination ratio [SiD]/([SiD] + [SiH]) and the D_2O concentration (0, 5, 10, 15, and 20%) was constructed [Fig. 2(c)]. Both estimations were performed for a 1-μm-thick layer from the surface of the film (2-μm-thick film), and the D profile of the SIMS data was averaged over the same 1-μm-thick layer. Both measurements showed that the D termination ratio on

TABLE I. Vibrational energies of Si-D and Si-H terminations. Theoretically calculated and experimentally observed values for the Si-H (111) and Si-D (111) vibrational energies are given for comparison [35–39]. NO denotes not observed in previous studies.

	Si-H observed	Si-D observed	Si-H (111)	Si-D (111)	Si-H calcd	Si-D calcd
1B	485	410	NO	415	476	412
2B	650	540	626	537	628	520
1S	485	485	NO	NO	480	480
2S	2100	1525	2083	1516	2120	1525

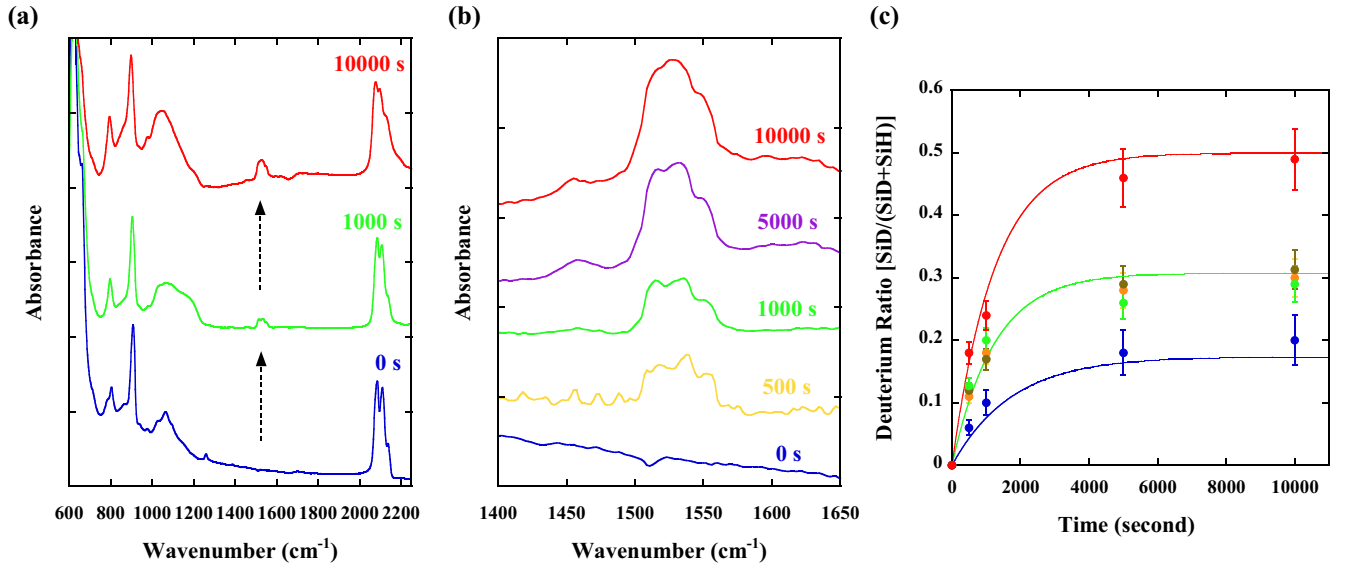

FIG. 3. Deuterium enrichment. (a) Absorbance spectra as a function of dipping duration (0 s: blue, 1000 s: green, 10 000 s: red). (b) Detailed attenuated total reflectance (ATR) spectra of Si-D stretching mode as a function of dipping duration (0 s: blue, 500 s: yellow, 1000 s: green, 5000 s: purple, 10 000 s: red). (c) D termination ratio as a function of dipping duration in 5% [blue circles: reflection-Fourier transform infrared (R-FTIR)], 10% (green circles: ATR-FTIR, brown circles: R-FTIR), and 20% (red circles: R-FTIR) D_2O solutions obtained from FTIR absorbance. For comparison, the secondary ion mass spectrometry (SIMS) data points obtained in 10% D_2O solution are shown (orange circles). The theoretically calculated lines that describe the D termination ratio [SiD]/([SiD] + [SiH]) as a function of dipping duration for 5% (blue line), 10% (green line), and 20% (red line) D_2O solution were fitted using reaction rates of $k_H = 2 \times 10^{-3}\,\mathrm{cm}^3/\mathrm{s}$ and $k_D = 5 \times 10^{-4}\,\mathrm{cm}^3/\mathrm{s}$.

n-Si is linearly proportional to the D_2O concentration. This linear correlation indicates that FTIR absorbance measurements can be used to obtain a quantitative estimate of the D termination ratio.

III. H-TO-D EXCHANGE REACTION EXPERIMENTS

Using standard samples for which the D termination ratios had been determined by both FTIR and SIMS, we performed exchange reaction experiments. Here, H-to-D exchange was performed by dipping the n-Si:H films into a mixed D_2O-HF-ethanol solution $[HF/H_2O/D_2O/C_2H_5OH = 25 : 25 + (20-\xi) : \xi : 30]$, where the volume of D_2O, denoted by ξ, was varied from 0 to 20% (0, 5, 10, and 20%). Figure 3(a) shows the absorbance spectra as a function of dipping duration (0 s: blue, 1000 s: green, and 10 000 s: red). By dipping the n-Si:H film into a 10% D_2O-HF-ethanol solution ($\xi = 10\%$), H termination was partially replaced by D termination. The replacement ratio increased with increasing dipping duration, as shown by the spectral growth of the Si-D stretching mode (1480–1570 cm^{-1}) indicated by the dotted arrows. The detailed FTIR spectra of the Si-D stretching mode as a function of dipping duration shown in Fig. 3(b) clearly reveals the time evolution of D termination enrichment. That is, when n-Si:H was dipped into a dilute 10% D_2O solution, the intensity corresponding to D termination rapidly increased over the first 1000 s. Subsequently, the rate of increase decreased and saturation occurred at ~5000–10 000 s. Plotting the D termination ratio, obtained by ATR-FTIR (green circles), R-FTIR (orange circles), and SIMS (brown circles), as a function of dipping duration [Fig. 3(c)] clearly revealed that the D termination ratio exceeded 30% despite using a 10% D_2O solution. This experimental result provides strong evidence that D isotope enrichment occurred on the surface of n-Si.

Based on previous studies [37,40–43] in which the D or H termination on Si was supplied from water, we considered the exchange reaction as $SiH + HDO \rightleftarrows SiD + H_2O$. Here, we define the rate of this reaction from left to right as k_H and from right to left as k_D. In this case, the rates of Si-D and Si-H formation are expressed as $d[SiD]/dt = k_H[SiH][HDO] - k_D[SiD][H_2O]$ and $d[SiH]/dt = -k_H[SiH][HDO] + k_D[SiD][H_2O]$, respectively, where [SiD] and [SiH] are the densities of Si-D and Si-H terminations (cm^{-2}) and [HDO] and [H_2O] are the concentrations of HDO and H_2O per volume (cm^{-3}). The D termination ratio [SiD]/([SiD] + [SiH]) can be obtained by solving both differential equations. The theoretical line that describes the D termination ratio is well fitted by reaction rates of $k_H = 2 \times 10^{-3}\,\mathrm{cm}^3/\mathrm{s}$ and $k_D = 5 \times 10^{-4}\,\mathrm{cm}^3/\mathrm{s}$, as shown by the solid green line in Fig. 3(c). Based on this theoretical fitting, we found that the exchange reaction from left to right proceeds four times faster than that from right to left. Here, we note that D atoms are supplied from HDO water molecules. As a path to D termination, HDO and/or DF contribute to the exchange reaction. In this case, it is likely that D termination originates from DF; however, in the reaction $HF + D_2O \rightleftarrows DF + HDO$, the enthalpy of this process is $\Delta H = -0.65\,\mathrm{kJ/mol}$ [44–46], resulting in a weak exothermic reaction. In contrast, in the reaction $D_2O + H_2O \rightleftarrows 2HDO$, the enthalpy is $\Delta H = -3.1\,\mathrm{kJ/mol}$ [45,46], resulting in a strong exothermic reaction. Therefore, we consider D atoms to be supplied by HDO molecules.

To confirm this reaction model, we performed D_2O concentration-dependent experiments. Figure 3(c) shows the

TABLE II. Zero-point oscillation energies, entropies, and the chemical potentials of Si-D and Si-H terminations. These values were calculated at $T = 300$ K. These values are given in kJ/mol.

	2S	1S	2B	1B	Entropy	Chemical potential
SiD	18.33	5.79	6.46	4.92	3.28	20.27
SiH	25.08	5.79	7.62	5.79	2.66	26.88

D termination ratio (determined by FTIR absorbance) as a function of dipping duration in 5% (blue circles) and 20% (red circles) D_2O solutions in addition to the 10% D_2O solution. The theoretically calculated lines fitted using the above-determined reaction rates describe all the behaviors of the D termination process. However, some systematic discrepancies between the experimental results and the theoretically calculated lines at lower (5%) or higher (20%) concentrations indicate that k_H and k_D are not constant but have some concentration dependence. However, we will not consider this concentration dependence of the reaction rates in detail because we are interested in the enrichment of naturally existing rare D elements.

IV. QUANTUM THEORY OF ISOTOPE EXCHANGE REACTION RATES

Based on the theory of chemical kinetics [47,48], the ratio of the reaction rates k_H/k_D can be expressed as $k_H/k_D = (\theta_H/\theta_D)\exp[-(\Delta G)/(RT)]$. In this equation, R is the gas constant, T is the temperature (K), θ_H and θ_D are parameters that depend on both the vibrational frequency and the temperature, and ΔG (kJ/mol) is the difference in the chemical potential before and after the reaction, described as $\Delta G = \mu_{SiD} + \mu_{H2O} - \mu_{SiH} - \mu_{HDO}$. In this equation, μ_{SiD} is expressed based on the quantum mechanical zero-point oscillation and the entropy terms as [47,48]

$$\mu_{SiD} = \sum_i \left\{ \left(\frac{1}{2}\hbar\omega_i^{SiD}\right) - RT \ln\left[1 + \exp\left(\frac{\hbar\omega_i^{SiD}}{RT}\right)\right] - \frac{\hbar\omega_i^{SiD}}{\left[\exp\left(\frac{\hbar\omega_i^{SiD}}{RT}\right) + 1\right]} \right\}, \quad (1)$$

where the sum denoted by i includes all the Si-D vibrational modes ($\hbar\omega_i$) such as bending and stretching modes. The μ_{SiH} term can be calculated by replacing D with H. The chemical potential of water is known to be $\mu_{H2O} = -237.2$ kJ/mol and $\mu_{HDO} = -241.9$ kJ/mol [44–46]. The zero-point oscillation energies, entropies, and the chemical potentials obtained from the above calculation are summarized in Table II, where each value is given in units of kJ/mol, and the values are calculated at $T = 300$ K. The value of the zero-point oscillation energy used here was based on the values determined by INS measurements. Finally, the difference in the free energy ΔG was estimated to be -1.88 kJ/mol. From this value, we evaluated the θ_H/θ_D ratio to be 2 based on kinetic isotope analysis [49,50] and Streitwieser's approximation [51]. By substituting these values (ΔG and θ_H/θ_D) into Eq. (1), the k_H/k_D ratio was determined to be 4.2, which coincides with the experimentally observed ratio of 4. We note here that, if the effect of the bending modes is excluded, which is generally omitted for the evaluation of isotope exchange reaction rates [48,52], k_H/k_D becomes 1.6. Therefore, we consider the bending modes to play a crucial role in the high rate for the isotope exchange reaction on the surface of n-Si.

V. PROTOCOLS FOR D ENRICHMENT ON n-Si

For isotope exchange reaction experiments performed in the liquid phase, we attained a fourfold increase in the D adatom concentration. This enrichment factor agreed well with the theoretical value estimated by considering the zero-point oscillation energies of the surface bending modes as well as the stretching modes. If we consider the replacement of D adatoms on the surface of n-Si:H in the gas phase, such as in a mixture of H_2 and HD, a much higher D adatom concentration is theoretically obtained based on the analysis in Sec. IV. The difference in the chemical potential before and after the reaction in the H_2 and HD gas phase can be described as $\Delta G = \mu_{SiD} + \mu_{H2} - \mu_{SiH} - \mu_{HD}$. For this theoretical calculation, the μ_{SiD} and μ_{SiH} values in Table II can be used, and the chemical potentials of H_2 and HD gas are known to be $\mu_{H2} = 0$ kJ/mol and $\mu_{HD} = -1.46$ kJ/mol [44–46]. Thus, the difference in free energy ΔG in the gas phase is estimated to be -5.12 kJ/mol, which is larger than that in the liquid phase. Moreover, this value gives a high separation ratio k_H/k_D of 15.6. We note here that this value coincides with the previous calculation for a Si surface [53].

Here, we propose a gas phase enrichment scheme using n-Si. Figure 4 shows protocols for D enrichment on the surface of n-Si in both liquid and gas phases. As shown in Fig. 4(a) for a natural water system, naturally occurring D isotopes (0.015% [54]) can be concentrated on the surface at a degree of ~0.06%. The n-Si used in this experiment contains $\sim 2.1 \times 10^{22}$ H atoms/g [55]. Therefore, this process captures 1.3×10^{19} D atoms/g on the surface of n-Si. Next, to enrich the D atoms, the gas phase reaction is considered. For example, upon transferring n-Si to a vacuum chamber, the H and D adatoms on the surface can be desorbed by heating. To desorb the D and H atoms from the surface, it is necessary to heat n-Si from 300 to ~600 K [56–58]. As shown in Fig. 4(b), the desorbed gas with a D concentration of 0.06% is concentrated to ~0.94%. After reheating to desorb and adsorb the D and H atoms, as shown in Fig. 4(c), the concentration of D adatoms becomes ~15%. We consider this simple exchange process on the surface of n-Si to offer sustainable, economical, and environmentally friendly D enrichment protocols. To realize this enrichment protocol efficiently, it is necessary to reduce the activation energy for the dissociation of H_2 on Si surface. Gas-phase enrichment using n-Si is currently under investigation and will be reported elsewhere.

VI. CONCLUSIONS AND OUTLOOK

We have demonstrated an efficient exchange reaction from H to D termination on the surface of n-Si to achieve a fourfold enrichment of D termination. The physical mechanism of D enrichment on n-Si was clarified based on QMCIE, and the difference in the zero-point oscillation energies and entropies

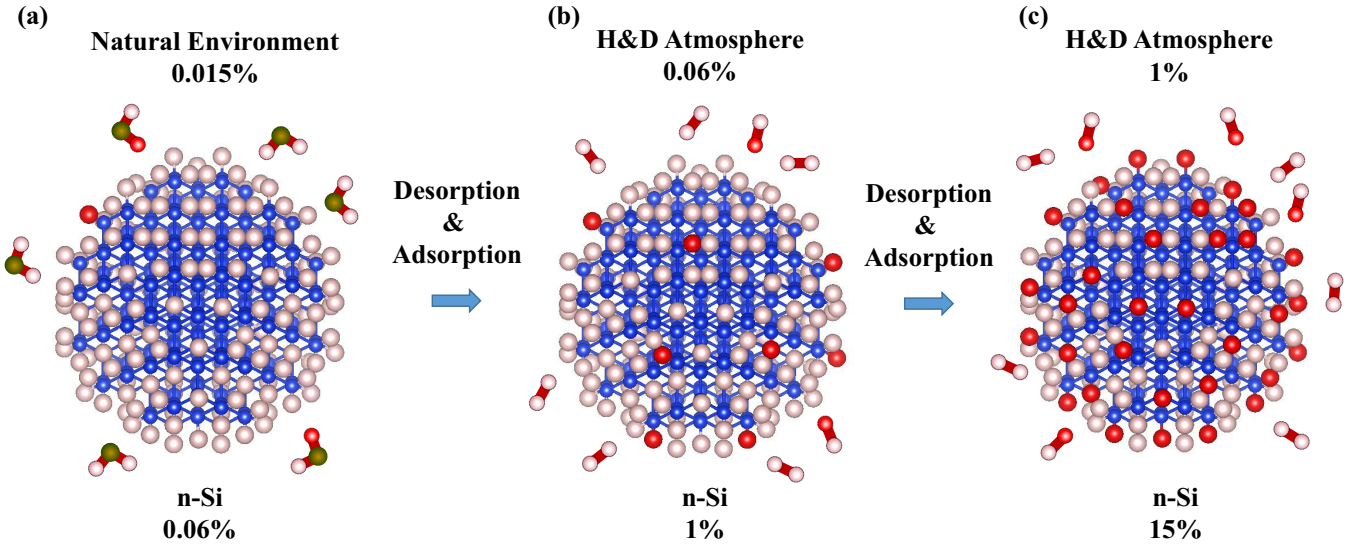

FIG. 4. Proposed deuterium enrichment protocol using n-Si (the pink, blue, red, and green atoms correspond to H, Si, D, and O, respectively). (a) D enrichment occurring in natural water. Naturally occurring D atoms (0.015%) can be concentrated on the surface to a degree of ∼0.06%. (b) n-Si is transferred to a vacuum chamber, and then H and D adatoms on the surface are desorbed by heating. The desorbed gas with a D concentration of 0.06% is enriched to a degree of ∼1% in the gas phase. (c) Second desorption and adsorption treatment. The D concentration is increased to a degree of ∼15% in the gas phase.

of the surface-localized vibrations between Si-H and Si-D was found to be crucial for this efficient exchange reaction. Similarly, the enrichment for other group IV semiconductors can be estimated, e.g., as 2.1 for C (diamond) and 2.8 for Ge using previously reported values for the vibrational energies of C-D [59,60], C-H [61–63], Ge-D [6,7,64–66], and Ge-H [6,7,64–66]. The theoretically estimated enhancement factors for C and Ge are smaller than those for Si, which can be understood from the difference in the energy between the bending modes and the bulk phonon frequency. That is, C has a higher bulk phonon frequency than the bending modes of C-H and C-D, and only the stretching mode contributes to the chemical potential. In contrast, Ge has a lower bulk phonon frequency than the Ge-H and Ge-D bending modes; therefore, both bending modes show a localized vibrational character. A much higher exchange reaction rate can be expected by using the antibonding state of Si-H (6–7 eV) because an extremely large isotope effect is observed on the Si surface [3,4]. Thus, the exchange reaction occurring on the surface of n-Si offers simple and economical D enrichment protocols.

Finally, we note here that tunneling effects are generally not considered in primary exchange reaction processes [52,53,67]. However, this phenomenon is known to greatly influence H-D substitution effects in chemistry [23,67–69]. The exchange reaction rate deviating from classical behavior may appear as a nonlinear Arrhenius plot at a low-temperature regime, and this is now under investigation.

ACKNOWLEDGMENTS

The authors thank Prof. N. Katayama (Nagoya City University) for providing access to FTIR equipment. T.M. thanks Dr. R. Miyagawa (Nagoya Institute of Technology) for assistance with the SIMS measurements as well as Dr. J. Suzuki (J-PARC) and Prof. M. Ohnuma (Hokkaido University) for help with the SAXS measurements. T.O. thanks Prof. S. M. Bennington for assistance with the INS measurements. This paper was supported by JSPS KAKENHI Grant No. 20H04455 and the Collaborative Research Program of the Institute for Chemical Research, Kyoto University (Grant No. 2020-97).

[1] A. Vértes, S. Nagy, Z. Klencsár, and R. G. Lovas, *Handbook of Nuclear Chemistry* (Kluwer Academic Publishers, Amsterdam, 2003).

[2] T. -C. Shen, C. Wang, G. C. Abeln, J. R. Tucker, J. W. Lyding, P. Avouris, and R. E. Walkup, Atomic-scale desorption through electronic and vibrational excitation mechanisms, Science **268**, 1590 (1995).

[3] Ph. Avouris, R. E. Walkup, A. R. Rossi, T.-C. Shen, G. C. Abeln, J. R. Tucker, and J. W. Lyding, STM-induced H atom desorption from Si(100): Isotope effects and site selectivity, Chem. Phys. Lett. **257**, 148 (1996).

[4] E. T. Foley, A. F. Kam, J. W. Lyding, and Ph. Avouris, Cryogenic UHV-STM Study of Hydrogen and Deuterium Desorption from Si(100), Phys. Rev. Lett. **80**, 1336 (1998).

[5] J. W. Lyding, K. Hess, G. C. Abeln, D. S. Thompson, J. S. Moore, M. C. Hersam, E. T. Foley, J. Lee, Z. Chen, S. T. Hwang, H. Choi, Ph Avouris, and I. C. Kizilyalli, Ultrahigh vacuum-scanning tunneling microscopy nanofabrication and hydrogen/deuterium desorption from silicon surfaces: Implications for complementary metal oxide semiconductor technology, Appl. Surf. Sci. **130–132**, 221 (1998).

[6] C. G. Van de Walle and W. B. Jackson, Comment on "Reduction of hot electron degradation in metal oxide semiconductor transistors by deuterium processing," Appl. Phys. Lett. **69**, 2441 (1996).

[7] C. G. Van de Walle, Hydrogen in silicon: Fundamental properties and consequences for devices, J. Vac. Sci. Technol. A **16**, 1767 (1998).

[8] R. Biswas, Y.-P. Li, and B. C. Pan, Enhanced stability of deuterium in silicon, Appl. Phys. Lett. **72**, 3500 (1998).

[9] J. W. Lyding, K. Hess, and I. C. Kizilyalli, Reduction of hot electron degradation in metal oxide semiconductor transistors by deuterium processing, Appl. Phys. Lett. **68**, 2526 (1996).

[10] K. Hess, I. C. Kizilyalli, and J. W. Lyding, Giant isotope effect in hot electron degradation of metal oxide silicon devices, IEEE Trans. Electron Devices **45**, 406 (1998).

[11] J. Lee, K. Cheng, Z. Chen, K. Hess, J. W. Lyding, Y. Kim, H. Lee, Y. Kim, and K. Suh, Application of high pressure deuterium annealing for improving the hot carrier reliability of CMOS transistors, IEEE Electron Device Lett. **21**, 221 (2000).

[12] T. Kundu and D. Misra, Enhanced SiO_2 reliability on deuterium-implanted silicon, IEEE Trans. Device Mater. Reliab. **6**, 288 (2006).

[13] J. Mizseia, E. Pap, K. Gillemotb, and G. Battistig, Effect of deuterium on passivation of Si surfaces, Appl. Surf. Sci. **256**, 5765 (2010).

[14] M. Schnabel1, B. W. H. van de Loo, W. Nemeth, B. Macco, P. Stradins, W. M. M. Kessels, and D. L. Young, Hydrogen passivation of poly-Si/SiO_x contacts for Si solar cells using Al_2O_3 studied with deuterium, Appl. Phys. Lett. **112**, 203901 (2018).

[15] H. K. Rae, *Separation of Hydrogen Isotopes* (ACS Symposium Series, Washington, DC, 1978), Chap. 1, pp. 1–26.

[16] W. B. Mann and W. C. Newell, The exchanges of energy between a platinum surface and hydrogen and deuterium molecules, Proc. R. Soc. A **158**, 397 (1937).

[17] A. Azua, S. Sanz, and E. Peris, Water-soluble Ir^{III}N-heterocyclic carbene based catalysts for the reduction of CO_2 to formate by transfer hydrogenation and the deuteration of aryl amines in water, Chem. Eur. J. **17**, 3963 (2011).

[18] J. L. Carriker, P. S. Wagenknecht, M. A. Hosseini, and P. E. Fleming, Transition metal catalyzed D_2/H_2O exchange: distinguishing between the single and double exchange pathways, J. Mol. Catal. A **267**, 218 (2007).

[19] G. Kovács, L. Nádasdi, G. Laurenczy, and F. Joó, Aqueous organometallic catalysis. Isotope exchange reactions in H_2-D_2O and D_2-H_2O systems catalyzed by water-soluble Rh- and Ru-phosphine complexes, Green. Chem. **5**, 213 (2003).

[20] F. A. Jalón, B. R. Manzano, A. Caballero, M. C. Carrión, L. Santos, G. Espino, and M. Moreno, Facile Ru-H_2 heterolytic activation and intramolecular proton transfer assisted by basic N-centers in the ligands, J. Am. Chem. Soc. **127**, 15364 (2005).

[21] P. V. Grundler, O. V. Yazyev, N. Aebischer, L. Helm, G. Laurenczy, and A. E. Merbach, Kinetic studies on the first dihydrogen aquacomplex, $[Ru(H_2)(H_2O)_5]^{2+}$: Formation under H_2 pressure and catalytic H/D isotope exchange in water, Inorg. Chim. Acta **359**, 1795 (2006).

[22] P. M. Vignais, H/D exchange reactions and mechanistic aspects of the hydrogenases, Coord. Chem. Rev. **249**, 1677 (2005).

[23] K. Mori, Y. Futamura, S. Masuda, H. Kobayashi, and H. Yamashita, Controlled release of hydrogen isotope compounds and tunneling effect in the heterogeneously-catalyzed formic acid dehydrogenation, Nat. Commun. **10**, 4094 (2019).

[24] T. Kurita, F. Aoki, T. Mizumoto, T. Maejima, H. Esaki, T. Maegawa, Y. Monguchi, and H. Sajiki, Facile and convenient method of deuterium gas generation using a Pd/C-catalyzed H_2-D_2 exchange reaction and its application to synthesis of deuterium-labeled compounds, Chem. Eur. J. **14**, 3371 (2008).

[25] W. Doster, S. Cusack, and W. Petry, Dynamical transition of myoglobin revealed by inelastic neutron scattering, Nature **337**, 754 (1989).

[26] T. Yildirim, O. Gülseren, J. W. Lynn, C. M. Brown, T. J. Udovic, Q. Huang, N. Rogado, K. A. Regan, M. A. Hayward, J. S. Slusky, T. He, M. K. Haas, P. Khalifah, K. Inumaru, and R. J. Cava, Giant Anharmonicity and Nonlinear Electron-Phonon Coupling in MgB_2: A Combined First-Principles Calculation and Neutron Scattering Study, Phys Rev. Lett. **87**, 037001 (2001).

[27] A. D. Christianson, E. A. Goremychkin, R. Osborn, S. Rosenkranz, M. D. Lumsden, C. D. Malliakas, I. S. Todorov, H. Claus, D. Y. Chung, M. G. Kanatzidis, R. I. Bewley, and T. Guidi, Unconventional superconductivity in $Ba_{0.6}K_{0.4}Fe_2As_2$ from inelastic neutron scattering, Nature **456**, 930 (2008).

[28] L. Hong, N. Jain, X. Cheng, A. Bernal, M. Tyagi, and J. C. Smith, Determination of functional collective motions in a protein at atomic resolution using coherent neutron scattering, Sci. Adv. **2**, e1600886 (2016).

[29] L. T. Canham, Silicon quantum wire array fabrication by electrochemical and chemical dissolution of wafers, Appl. Phys. Lett. **57**, 1046 (1990).

[30] T. Matsumoto, J. Suzuki, M. Ohnuma, Y. Kanemitsu, and Y. Masumoto, Evidence of quantum size effect in nanocrystalline silicon by optical absorption, Phys. Rev. B **63**, 195322 (2001).

[31] G. Porod, in *Small-Angle X-Ray Scattering*, edited by O. Glatter and O. Kratky (Academic Press, London, 1982), p. 17.

[32] A. I. Belogorokhov, S. A. Gavrilov, P. K. Kashkarov, and I. A. Belogorokhov, FTIR investigation of porous silicon formed in deutrofluoric acid based solutions, Phys. Stat. Sol. **202**, 1581 (2005).

[33] T. Matsumoto, A. I. Belogorokhov, L. I. Belogorokhova, Y. Masumoto, and E. A. Zhukov, The effect of deuterium on the optical properties of free-standing porous silicon layers, Nanotechnology **11**, 340 (2000).

[34] A. J. Dianoux and G. Lander, *Neutron Data Booklet* (Institut Laue-Langevin, Grenoble, 2003).

[35] T. Matsumoto, T. Ohhara, H. Sugimoto, S. M. Bennington, and S. Ikeda, Quantum twin spectra in nanocrystalline silicon, Phys. Rev. Materials **1**, 051601 (2017).

[36] G. A. Ferguson, K. Raghavachari, D. J. Michalak, and Y. Chabal, Adsorbate−surface phonon interactions in deuterium-passivated Si(111)-(1 × 1), J. Phys. Chem. C **112**, 1034 (2008).

[37] S. Watanabe, Isotopic shift and broadening of Si-D bending vibration on Si(111), Appl. Surf. Sci. **162–163**, 146 (2000).

[38] B. Sandfort, A. Mazur, and J. Pollmann, Surface phonons of hydrogen-terminated semiconductor surfaces. I. The H:Si(111)-(1 × 1) surface, Phys. Rev. B **51**, 7139 (1995).

[39] V. Gräschus, A. Mazur, and J. Pollmann, Surface phonons of D:Si(111)−(1 × 1), Surf. Sci. **368**, 179 (1996).

[40] V. A. Burrows, Y. J. Chabal, G. S. Higashi, K. Raghavachari, and S. B. Christman, Infrared spectroscopy of Si(111) surfaces

after HF treatment: hydrogen termination and surface morphology, Appl. Phys. Lett. **53**, 998 (1988).

[41] S. Watanabe, Infrared investigation of deuterated Si(111) surface formed in hot heavy water, Appl. Phys. Lett. **67**, 3620 (1995).

[42] H. Luo and C. E. D. Chidsey, D-Si(111)(1 × 1) surface for the study of silicon etching in aqueous solutions, Appl. Phys. Lett. **72**, 477 (1998).

[43] P. Jakob, Y. J. Chabal, K. Raghavachari, R. S. Becker, and A. J. Becker, Kinetic model of the chemical etching of Si(111) surfaces by buffered HF solutions, Surf. Sci. **275**, 407 (1992).

[44] D. R. Stull and H. Prophet, *JANAF Thermochemical Tables* (National Bureau of Standards, Washington, DC, 1971).

[45] G. Job and F. Herrmann, Chemical potential—a quantity in search of recognition, Eur. J. Phys. **27**, 353 (2006).

[46] D. D. Wagman, W. H. Evans, V. B. Parker, R. H. Schumm, I. Halow, S. M. Bailey, K. L. Churney, and R. L. Nuttall, The NBS tables of chemical thermodynamic properties. Selected values for inorganic and C_1 and C_2 organic substances in SI units, J. Phys. Chem. Ref. Data **11**, Suppl. 2 (1982).

[47] H. Eyring, The activated complex in chemical reactions, J. Chem. Phys. **3**, 107 (1935).

[48] O. P. Chikalova-Luzina and T. Matsumoto, Ratio of deuterium to hydrogen termination on silicon surface in aqueous electrolyte solutions, Appl. Phys. Lett. **80**, 4507 (2002).

[49] O. Redlich, A general relationship between the oscillation frequency of isotropic molecules, Z. Phys. Chem. **28B**, 371 (1935).

[50] J. Bigeleisen and M. G. Mayer, Calculation of equilibrium constants for isotopic exchange reactions, J. Chem. Phys. **15**, 261 (1947).

[51] A. Streitwieser, R. H. Jagow, R. C. Fahey, and S. Suzuki, Kinetic isotope effects in the acetolyses of deuterated cyclopentyl tosylates, J. Am. Chem. Soc. **80**, 2326 (1958).

[52] L. Melander, *Isotope Effects of Reaction Rates* (The Ronald Press Company, New York, 1960).

[53] I. P. Ipatova, O. P. Chikalova-Luzina, and K. Hess, Effect of localized vibrations on the Si surface concentrations of H and D, J. Appl. Phys. **83**, 814 (1998).

[54] R. Hagemann, G. Nief, and E. Roth, Absolute isotopic scale for deuterium analysis of natural waters. Absolute D/H ratio for SMOW, Tellus. **22**, 712 (1970).

[55] V. Lysenko, F. Bidault, S. Alekseev, V. Zaitsev, D. Barbier, C. Turpin, F. Geobaldo, P. Rivolo, and E. Garrone, Study of porous silicon nanostructures as hydrogen reservoirs, J. Phys. Chem. B **109**, 19711 (2005).

[56] P. Gupta, V. L. Colvin, and S. M. George, Hydrogen desorption kinetics from monohydride and dihydride species on silicon surfaces, Phys. Rev. B **37**, 8234 (1988).

[57] S. M. Prokes, O. J. Glembocki, V. M. Bermudez, R. Kaplan, L. E. Friedersdorf, and P. C. Searson, SiH_x excitation: An alternate mechanism for porous Si photoluminescence, Phys. Rev. B **45**, 13788(R) (1992).

[58] H. Shinoda, T. Nakajima, K. Ueno, and N. Koshida, Thermally induced ultrasonic emission from porous silicon, Nature **400**, 853 (1999).

[59] T. Aizawa, T. Ando, K. Yamamoto, M. Kamo, and Y. Sato, Surface vibrational studies of CVD diamond, Diamond Relat. Mater. **4**, 600 (1995).

[60] A. Glebov, J. P. Toennies, S. Vollmer, S. A. Safron, J. G. Skofronick, V. Gräschus, A. Mazur, and J. Pollmann, Phonon dynamics and structure of the deuterated diamond(111)-(1 × 1) surface: Experiment and theory, Phys. Rev. B **57**, 10082 (1998).

[61] S. Lee and G. Apai, Surface phonons and CH vibrational modes of diamond (100) and (111) surfaces, Phys. Rev. B **48**, 2684 (1993).

[62] T. Aizawa, T. Ando, M. Kamo, and Y. Sato, High-resolution electron-energy-loss spectroscopic study of epitaxially grown diamond (111) and (100) surfaces, Phys. Rev. B **48**, 18348(R) (1993).

[63] B. Sandfort, A. Mazur, and J. Pollmann, Surface phonons of hydrogen-terminated semiconductor surfaces. II. The H:C(111)-(1 × 1) system, Phys. Rev. B **51**, 7150 (1995).

[64] G. A. N. Connell and J. R. Pawlik, Use of hydrogenation in structural and electronic studies of gap states in amorphous germanium, Phys. Rev. B **13**, 787 (1976).

[65] X. Han, T. Balgar, and E. Hasselbrinka, Vibrational dynamics of hydrogen on Ge surfaces, J. Chem. Phys. **130**, 134701 (2009).

[66] L. Papagno, X. Y. Shen, J. Anderson, G. Schirripa Spagnolo, and G. J. Lapeyre, Hydrogen adsorption on Ge(100) studied by high-resolution energy-loss spectroscopy, Phys. Rev. B **34**, 7188 (1986).

[67] P. R. Schreiner, Tunneling control of chemical reactions: The third reactivity paradigm, J. Am. Chem. Soc. **139**, 15276 (2017).

[68] R. J. McMahon, Chemical reactions involving quantum tunneling, Science **299**, 833 (2003).

[69] J. Meisner and J. Kästner, Atom tunneling in chemistry, Angew. Chem. Int. Ed. **55**, 5400 (2016).